

Supplementary Information

Kinetic Friction of Structurally Superlubric 2D Material Interfaces

Jin Wang,^{1,2} Ming Ma,³ and Erio Tosatti^{1,2,4,*}

¹*International School for Advanced Studies (SISSA), I-34136 Trieste, Italy*

²*International Centre for Theoretical Physics, I-34151 Trieste, Italy*

³*State Key Laboratory of Tribology,*

Department of Mechanical Engineering,

Tsinghua University, Beijing 100084, China

⁴*CNR-IOM, Consiglio Nazionale delle Ricerche - Istituto*

Officina dei Materiali, c/o SISSA, 34136, Trieste, Italy

CONTENTS

I. Methods for structural optimization	2
II. Negligible effects from in-plane damping	2
III. Damping coefficient from anisotropic Debye model	3
IV. Thermal fluctuations from simulations	4
V. Corrugations with different k_z	5
References	7

* tosatti@sissa.it

I. METHODS FOR STRUCTURAL OPTIMIZATION

The energy optimization is performed with open-source code LAMMPS [1, 2]. The bilayer simulation models with twist angle θ ranges from 0.3° to 30° are created with periodic boundary conditions (PBC) along x and y directions. The interlayer and intralayer interaction is described by registry-dependent interlayer potential (ILP) and REBO force field respectively [3, 4]. The carbon atom in each layer is tethered by a linear z -directional spring to its original position to mimic the normal direction elasticity. The spring constant, which reproduces the moiré height in twisted bulk graphite, is $k_z = 0.33$ N/m. During the structural optimization, the in-plane stress is kept to be zero, $p_{xx} = p_{yy} = p_{xy} = 0$. The optimization is performed by FIRE [5] together with CG algorithms with several loops. The convergence criterion is when the largest single atom force $F_i < 10^{-6}$ eV/Å.

II. NEGLIGIBLE EFFECTS FROM IN-PLANE DAMPING

The in-plane damping ζ_x (and ζ_y) is negligible (compared to the out-of-plane ζ_z) in the damping-based bilayer graphene simulations. This has been realized before (e.g., Ref. [6]) and can be understood here by defining an anisotropy factor:

$$r_{aniso} = \frac{\zeta_z}{\zeta_x} = \frac{|\Phi_{12}^{zz}|^2}{|\Phi_{12}^{xx}|^2} \quad (\text{S1})$$

The z -direction force constant is $\Phi_{12}^{zz} = 2.7$ N/m (could also be estimated from elastic constant $C_{33} = 38.7$ GPa by $\Phi_{12}^{zz} = C_{33}A_C/d_0$), and the force constant Φ_{12}^{xx} could be estimated from the interlayer shearing $C_{44} = 5.0$ GPa [7]. Since $\Phi_{12}^{zz}/\Phi_{12}^{xx} = C_{33}/C_{44}$, the anisotropy factor is in the order of 10^2 – the friction contribution from in-plane damping is thus negligible.

III. DAMPING COEFFICIENT FROM ANISOTROPIC DEBYE MODEL

Considering an anisotropic Debye model with dispersion relation [8]:

$$\omega^2 = v_{\text{in}}^2(q_x^2 + q_y^2) + v_{\text{out}}^2 q_z^2 \quad (\text{S2})$$

where v_{in} and v_{out} is the in-plane and out-of-plane sound speed. The first Brillouin zone of this model is assumed to be an ellipsoid:

$$\left(\frac{q_x}{q_{x0}}\right)^2 + \left(\frac{q_y}{q_{y0}}\right)^2 + \left(\frac{q_z}{q_{z0}}\right)^2 = 1 \quad (\text{S3})$$

/here for 2D materials, we take $q_{x0} = q_{y0}$. The Debye frequencies along in-plane and out-of-plane directions could be defined as $\omega_{Dx} = \omega_{Dy} = v_{\text{in}} q_{x0}$ and $\omega_{Dz} = v_{\text{out}} q_{z0}$.

The density of state is [9]:

$$\begin{aligned} \rho(\omega) &= \frac{V}{8\pi^3} \int \frac{dS}{v_g} \\ &= 2 \times \frac{V}{8\pi^3} \iint \frac{1}{v_g} \sqrt{1 + \left(\frac{\partial q_z}{\partial q_x}\right)^2 + \left(\frac{\partial q_z}{\partial q_y}\right)^2} dq_x dq_y \end{aligned} \quad (\text{S4})$$

where V is the volume of the unit cell, $v_g = |\nabla_q \omega|$ is the magnitude of the group velocity of a phonon, S represents the surface “area” of the zone boundary. By implementing the polar coordinate substitution $q_x = r \cos \varphi$ and $q_y = r \sin \varphi$ ($r \in [0, \omega/v_{\text{in}}]$, $\varphi \in [0, 2\pi]$), one could simplify the above equation to

$$\rho(\omega) = \frac{V\omega^2}{2\pi^2 v_{\text{in}}^2 v_{\text{out}}} \quad (\text{S5})$$

This result holds for $\omega < \omega_{Dz}$ – consistent with our work. Substituting Eq. (S5) back into Eq. 23 in the maintext, we could get the damping coefficient:

$$\zeta_z = \frac{|\Phi_{12}^{zz}|^2}{m^2} \frac{V}{4\pi v_{\text{in}}^2 v_{\text{out}}} \quad (\text{S6})$$

By using sound speed $v_{\text{in}} = 22$ km/s and $v_{\text{out}} = 1.48$ km/s [7], one could get the damping coefficient $\zeta \approx 0.02$ ps⁻¹ – agree qualitatively with the estimation given in the main text.

IV. THERMAL FLUCTUATIONS FROM SIMULATIONS

In this section, we give details on the mean-square (out-of-plane) thermal fluctuation $\langle H_T^2 \rangle$ of the interfacial layer (region B) and its temperature dependence.

For bilayer graphene simulations (described in maintext Sect. 6.1), we can get trajectory of all atoms, $x_i(t)$, $y_i(t)$, and $z_i(t)$. According to definition,

$$\langle H_T^2 \rangle = \sum_q \langle |h_q|^2 \rangle \quad (\text{S7})$$

where $\langle |h_q|^2 \rangle$ could be estimated from 2D Fourier transform of $z(x, y)$:

$$\langle |h_q|^2 \rangle = \langle |\text{FFT}_q|^2 \rangle \quad (\text{S8})$$

here $|\dots|$ represents complex modulus, and

$$\text{FFT}(q_x, q_y) = \frac{4}{N_x N_y} \sum_{j=0}^{N_x-1} \sum_{k=0}^{N_y-1} \exp\left(-\frac{2\pi i q_x j}{N_x}\right) \exp\left(-\frac{2\pi i q_y k}{N_y}\right) z(x_j, y_k) \quad (\text{S9})$$

where $z(x_j, y_k)$ is the out-of-plane position of the substrate (or slider), remapping from the original honeycomb lattice to square lattice with spatial resolution $N_x \times N_y$.

The temperature dependence of $\langle H_T^2 \rangle$ (for $T > T_c$) is shown in Fig. S1a. Note that at low temperature limit ($T \rightarrow 0$), the mean-square-corrugation becomes H_{moire}^2 . For $\theta = 6^\circ$, it is approximately 10^{-2} \AA^2 . From simulation results, we can determine the value of c_2 by:

$$c_2 = \frac{\kappa \langle H_T^2 \rangle}{k_B T a_{\text{Gr}}^2} \approx 2.8 \quad (\text{S10})$$

where κ is the bending stiffness of monolayer graphene, a_{Gr} is the lattice constant of graphene. Substituting this c_2 back into Eq. (28) in the maintext, we find that the friction force estimated from our theory is in good agreement with the simulation results (Fig. 5d in the maintext).

The origin of this temperature dependence of friction (at high temperatures $T > T_c$) is $\langle H_T^2 \rangle$, as we formulate in Eq. (27) in the maintext. This could also be demonstrated directly from our simulation as shown in Fig. S1b. The errorbar of the friction force is the standard deviation of three independent simulations. Simulation results show that $F_{\text{norm}} = F_k a_{\text{Gr}}^2 (Nm \zeta_z v_0)^{-1} \simeq \langle H_T^2 \rangle$ at high temperatures, which lead immediately to:

$$F_k \simeq \frac{Nm \zeta_z \langle H_T^2 \rangle v_0}{a_{\text{Gr}}^2} \quad (\text{S11})$$

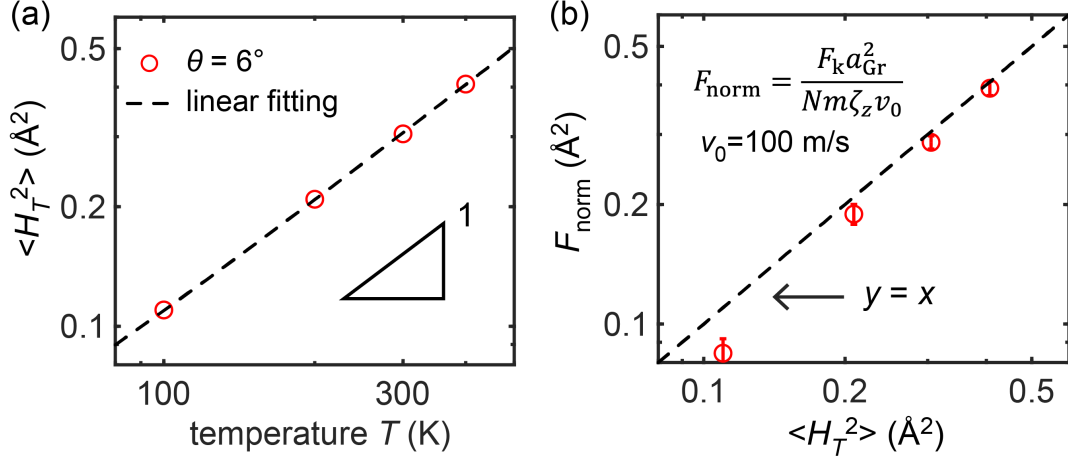


FIG. S1. (a) Temperature dependence of mean-square (out-of-plane) thermal fluctuations $\langle H_T^2 \rangle$. (b) A direct comparison between the “normalized friction” F_{norm} and $\langle H_T^2 \rangle$. Slope with $y = x$ is plotted as a guide for the eye.

V. CORRUGATIONS WITH DIFFERENT k_z

In the maintext, we use the same out-of-plane restriction k_z to slider and substrate. This set-up naturally gives rise to the same moiré height and thermal corrugations. In real nature there are cases where k_z is different for slider and substrate, e.g, graphite/hBN heterostructures, twisted monolayer graphene on Bernal graphite, etc. Discussions on fluctuations and sliding frictions for these variety of systems with “asymmetric” k_z will be given in this section.

At low temperature limit, the sliding friction is dominated by the moiré corrugation, i.e., Eq. (12) in the maintext. With different k_z for the substrate and slider, the moiré corrugation changes correspondingly. Thus, Eq. (12) could be generalized by defining H_{sub} and H_{sli} whose values can be determined by finding the global minimum potential energy. Here, instead, we show the simulation results of moiré corrugation for different slider’s k_z . Adopting the same optimization protocol with substrate’s $k_z = 0.33 \text{ N/m}$ and slider’s k_z ranging from 0 to 3 N/m, the moiré corrugations for the slider H_{sli} and substrate H_{sub} of a test case with 6° -twist bilayer graphene are shown in Fig. S2. From simulations, whether k_z of the slider is zero or equals to that of the substrate has weak influence on H_{sub} and negligible effect on the average moiré height $(H_{\text{sub}} + H_{\text{sli}})/2$. Therefore, it is safe to continue using Eq. (12) in the maintext to approximate the moiré corrugations for more general SSL

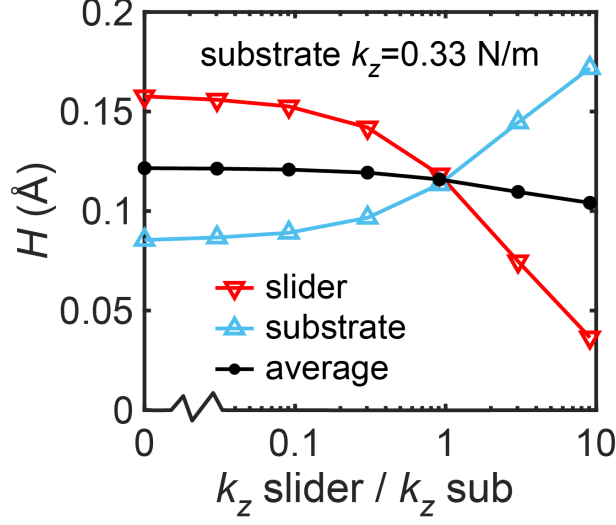


FIG. S2. Dependence of moiré corrugation on the ratio of slider to substrate k_z . The spring constant for the substrate is fixed to be $k_z = 0.33$ N/m.

systems.

For high temperature cases, where moiré fluctuations become negligible, the sliding friction is dominated by mean-square-fluctuations $\langle H_T^2 \rangle$. The larger k_z results in higher deformation energy, which leads to a decrease in $\langle H_T^2 \rangle$ (and the sliding friction) at the same temperature. We test on the parameter-free multilayer simulation system with two cases: k_z of the slider is equal to 0 and 0.33 N/m. From the simulation results shown in Fig. S3, the frictional stress at room temperature for $k_z = 0$ case (green) increased by $\approx 30\%$ compared to the finite k_z case (red). Simulation and theoretical results for the bilayer system with equal k_z are also shown in the figure.

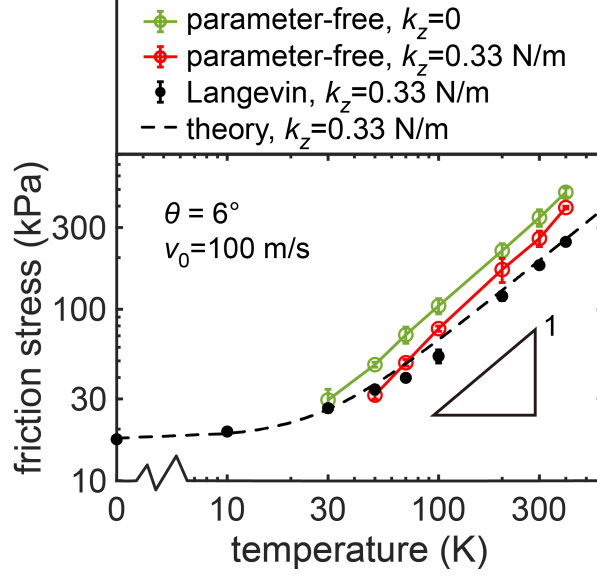


FIG. S3. Temperature dependence of frictional stress. Green and red circles: parameter-free simulation results for slider's k_z equal to 0 and 0.33 N/m. Black dots: Langevin-based simulation results (with ζ_z estimated from Eq. 24 in the maintext) for $k_z^{\text{sli}} = k_z^{\text{sub}} = 0.33$ N/m. Dashed line: theoretical estimation with $k_z^{\text{sli}} = k_z^{\text{sub}} = 0.33$ N/m.

-
- [1] Steve Plimpton. Fast parallel algorithms for short-range molecular dynamics. *Journal of Computational Physics*, 117(1):1–19, 1995.
 - [2] Aidan P. Thompson, H. Metin Aktulga, Richard Berger, Dan S. Bolintineanu, W. Michael Brown, Paul S. Crozier, Pieter J. in 't Veld, Axel Kohlmeyer, Stan G. Moore, Trung Dac Nguyen, Ray Shan, Mark J. Stevens, Julien Tranchida, Christian Trott, and Steven J. Plimpton. LAMMPS - a flexible simulation tool for particle-based materials modeling at the atomic, meso, and continuum scales. *Computer Physics Communications*, 271:108171, 2022.
 - [3] Wengen Ouyang, Davide Mandelli, Michael Urbakh, and Oded Hod. Nanoserpents: Graphene nanoribbon motion on two-dimensional hexagonal materials. *Nano Letters*, 18(9):6009–6016, 2018.
 - [4] Donald W Brenner, Olga A Shenderova, Judith A Harrison, Steven J Stuart, Boris Ni, and Susan B Sinnott. A second-generation reactive empirical bond order (rebo) potential energy expression for hydrocarbons. *Journal of Physics: Condensed Matter*, 14(4):783, 2002.

- [5] Erik Bitzek, Pekka Koskinen, Franz Gähler, Michael Moseler, and Peter Gumbsch. Structural relaxation made simple. *Phys. Rev. Lett.*, 97:170201, Oct 2006.
- [6] B.N.J Persson. *Sliding Friction, Physical Principles and Applications*. Springer, Berlin, 2000.
- [7] Alexey Bosak, Michael Krisch, Marcel Mohr, Janina Maultzsch, and Christian Thomsen. Elasticity of single-crystalline graphite: Inelastic x-ray scattering study. *Phys. Rev. B*, 75:153408, Apr 2007.
- [8] Z. Chen, Z. Wei, Y. Chen, and C. Dames. Anisotropic debye model for the thermal boundary conductance. *Phys. Rev. B*, 87:125426, Mar 2013.
- [9] Charles Kittel, Paul McEuen, and Paul McEuen. *Introduction to solid state physics*, volume 8. Wiley New York, 1996.